

Extremely Flexible Indium-Gallium-Zinc Oxide (IGZO) Based Electronic Devices Placed on an Ultrathin Poly(Methyl Methacrylate) (PMMA) Substrate

Yogeenth Kumaresan, Ryeri Lee, Namsoo Lim, Yusin Pak, Hyeonghun Kim, Woochul Kim, and Gun-Young Jung*

The flexibility of metal oxide-based electronic devices is severely limited by the thickness of their substrate. To enhance the flexibility of semiconducting metal oxide-based electronic devices, a new and simple way to fabricate indium-gallium-zinc oxide (IGZO)-based electronic devices on an ultrathin (1.9 μm) poly(methyl methacrylate) (PMMA) substrate is introduced. The PMMA layer spin-coated on an unmodified glass slide has no chemical interactions at the interface, resulting in weak adhesion. Therefore, the PMMA layer with the devices is readily peeled off the underlying glass slide without using any sacrificial layer. Thin film transistors (TFTs) and gas sensors are fabricated on a 1.9 μm thick PMMA substrate. The fabricated bottom-gated IGZO TFTs exhibits excellent transistor performances with a mobility of $10.7 \text{ cm}^2 \text{ V}^{-1} \text{ s}^{-1}$, a threshold voltage of 8.4 V and an on/off current ratio of 5×10^5 . The PMMA substrate having palladium (Pd)-decorated IGZO H_2 sensors is attached to the nonplanar substrates such as wrinkled hand glove and poly(vinyl chloride) (PVC) gas tubes, and the sensors demonstrate an excellent sensitivity of $\approx 10^6\%$ at 5% H_2 concentration at room temperature. Furthermore, both electronic devices show superior flexibility without any performance degradation even at a bending radius down to $<1 \text{ mm}$.

deformation is highly recommended for wearable electronics placed on any textile products and/or hand gloves.^[20,21] In general, the substrate having the electronic devices plays an important role in their flexibility. To date, polyimide (PI) has been widely utilized as a flexible substrate due to its excellent dielectric property, and good chemical and thermal stability.^[22–27] However, commercially available PI is not transparent, which limits its use in display applications, and conformal contact of PI substrate onto nonplanar surfaces such as gloves, flexible poly(vinyl chloride) (PVC) tubes, or cotton by using a glue is impractical.

To attain both high flexibility and conformal contact of electronic devices, researchers have designed free-standing organic devices, in which a polymer dielectric layer (e.g., polystyrene, polyacrylonitrile, polylactide) or organic active layer (e.g., pentacene) itself acts as a substrate.^[28–31] Zhang et al. fabricated free-

standing pentacene field effect transistors (FETs) by utilizing a polyacrylonitrile dielectric layer to hold the device components and attached it onto rough or even sharp substrates.^[32] However, as semiconducting polymers are not stable under atmospheric conditions,^[33,34] metal oxide-based electronic devices^[35–37] using thin inorganic semiconductor layers, such as SnO_2 , ZnO , In-Ga-ZnO , MoO_3 , and TiO_2 , are utilized; however, the thin metal oxide layers cannot endure physical strain greater than 1%, while being bent and twisted.^[38] In fact, the physical strain (S) acting on the thin metal oxide layer while being bent can be controlled by substrate thickness, which is determined by a simple formula $S = d/2r$ (" d " is the substrate thickness, and " r " is the bending radius).

Therefore, metal oxide-based electronic devices placed on top of an ultrathin organic substrate have been pursued to have less physical strain for ultraflexibility.^[39–43] Han et al. engineered a foldable indium tin oxide (ITO)-coated glass platform composed of thick and nondeformable parts surrounded by thin and foldable glass, which was selectively etched down to 5 μm , and successfully obtained a foldable substrate without any device failure.^[39] Hassan et al. utilized a thin Al_2O_3 substrate to fabricate flexible metal oxide-based H_2 sensors.^[40] Kim et al. fabricated In-Ga-ZnO TFTs on a 1.5 μm thick polyimide substrate and demonstrated its bendability at a bending radius down to 0.25 mm.^[41]

1. Introduction

The technological advancements in contemporary electronics, such as wearable computers, sensors, and flexible and rollable displays, demand electronic components placed on an arbitrary substrate to be bendable, foldable, twistable, and rollable.^[1–15] So far, there are many reports focusing on performance enhancement in various electronic devices, including sensors and thin film transistors (TFTs).^[16–19] However, maintaining device performance before and after extreme mechanical

Y. Kumaresan, R. Lee, N. Lim, H. Kim, W. Kim, Prof. G.-Y. Jung
School of Materials Science and Engineering
Gwangju Institute of Science and Technology (GIST)
123 Cheomdan-gwagiro, Buk-gu, Gwangju 61005, Republic of Korea
E-mail: gyjung@gist.ac.kr

Y. Pak
Physical Science and Engineering Division
King Abdullah University of Science and Technology (KAUST)
Thuwal 23955-6900, Saudi Arabia

 The ORCID identification number(s) for the author(s) of this article can be found under <https://doi.org/10.1002/aelm.201800167>.

DOI: 10.1002/aelm.201800167

However, handling these ultrathin substrates poses serious manufacturing challenges, including undesirable warping and fragility. Therefore, prior to the device fabrication process, the ultrathin substrate should be attached to a rigid substrate through a sacrificial layer.^[41–43] Ultimately, the ultrathin substrate having the devices is finally separated from the rigid substrate by mechanical detachment^[41,42] or by selective removal of the underlying sacrificial layer via a solution process through intentionally produced openings.^[43] However, easy separation over a large area is still a challenge in the use of a sacrificial layer.

In this paper, we introduced a simple and novel method to separate an ultrathin poly(methyl methacrylate, PMMA) layer having metal oxide-based electronic devices by engineering the surface energy between the PMMA layer and glass substrate. The adhesion of PMMA to the glass slide was studied with contact angle measurements and attenuated total reflection Fourier transform infrared (ATR-FTIR) spectroscopy. Bottom-gated indium-gallium-zinc oxide (IGZO) TFTs and palladium-decorated (Pd-dec) IGZO H₂ sensors were fabricated on top of the 0.7 μm negative resist/1.2 μm PMMA layers (hereafter, called as PMMA substrate, see Figure S1, Supporting Information). The devices were folded without nearly any device performance degradation, and made excellent conformal contact with nonplanar surfaces such as wrinkled hand gloves and flexible PVC gas tubes.

2. Results and Discussion

2.1. Free-Standing Ultrathin PMMA Substrate Preparation

Figure 1 presents the fabrication scheme for electronic devices, such as IGZO-based TFTs and IGZO-based H₂ sensors, on a

thin PMMA layer/glass slide and the subsequent separation of the electronic devices from the glass slide. The detailed explanation of the device fabrication and separation is given in the Experimental Section. We utilized two different glass slides, namely, an unmodified glass slide and a piranha-treated glass slide; the glass slides were cleaned using only isopropyl alcohol (IPA) or IPA and piranha (3 parts of concentrated sulfuric acid and 1 part of hydrogen peroxide) solution, respectively, prior to PMMA spin coating. The water contact angle and ATR-FTIR spectrum of both the unmodified glass slide and piranha-treated glass slide were measured to study the interfacial interaction of PMMA with the glass surface. As shown in Figure 2a–c, the contact angle of the unmodified glass slide, the piranha-treated glass slide, and the PMMA layer spin-coated over a glass slide were 45°, 9°, and 73°, respectively. In general, the adhesion of the PMMA film increases with the surface energy of glass slide.^[44] The smaller contact angle of the piranha-treated glass slide indicates that it had a higher surface energy than the unmodified glass slide and thus was in a less thermodynamically stable state, which favored the surface covering with other materials. Therefore, the adhesion of the PMMA layer to the piranha-treated glass slide was much stronger than that to the unmodified glass.

To analyze the chemical interaction of PMMA with the two different glass substrates at the interface, ATR-FTIR spectra of the unmodified glass slide, the piranha-treated glass slide, and the PMMA layer spin-coated on both the unmodified glass slide and the piranha-treated glass slide were measured at 2500–3400 cm⁻¹, as shown in Figure 2d,e. The broad peak at ≈3289 cm⁻¹ for the piranha-treated glass indicates a non-complexed (free) O-H band vibration, which was absent from the spectrum of the unmodified glass (Figure 2d), suggesting

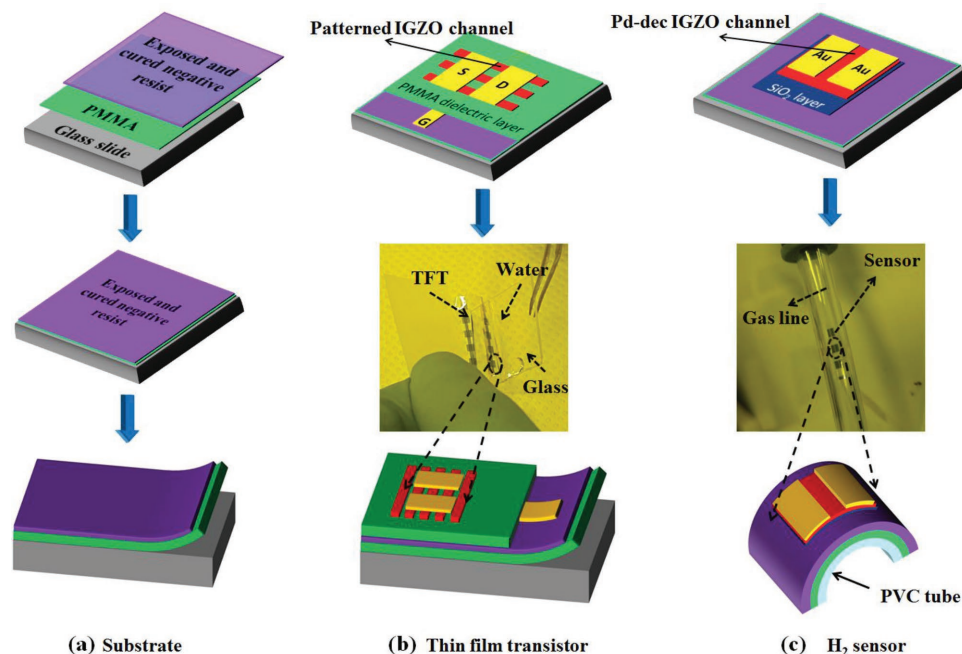


Figure 1. A schematic drawing representing the fabrication process for the flexible bottom-gated IGZO TFTs and the Pd-dec IGZO-based H₂-sensors on an ultrathin PMMA substrate; a) Ultrathin substrate preparation, b) bottom-gated IGZO TFT fabrication and separation of PMMA substrate from the glass slide, and c) Pd-dec IGZO-based H₂ sensor fabrication and attachment to a PVC gas tube. Digital images of IGZO TFTs during separation from the glass slide and Pd-dec IGZO-based H₂ sensor attached on a PVC gas tube are given in the middle row of (b) and (c), respectively.

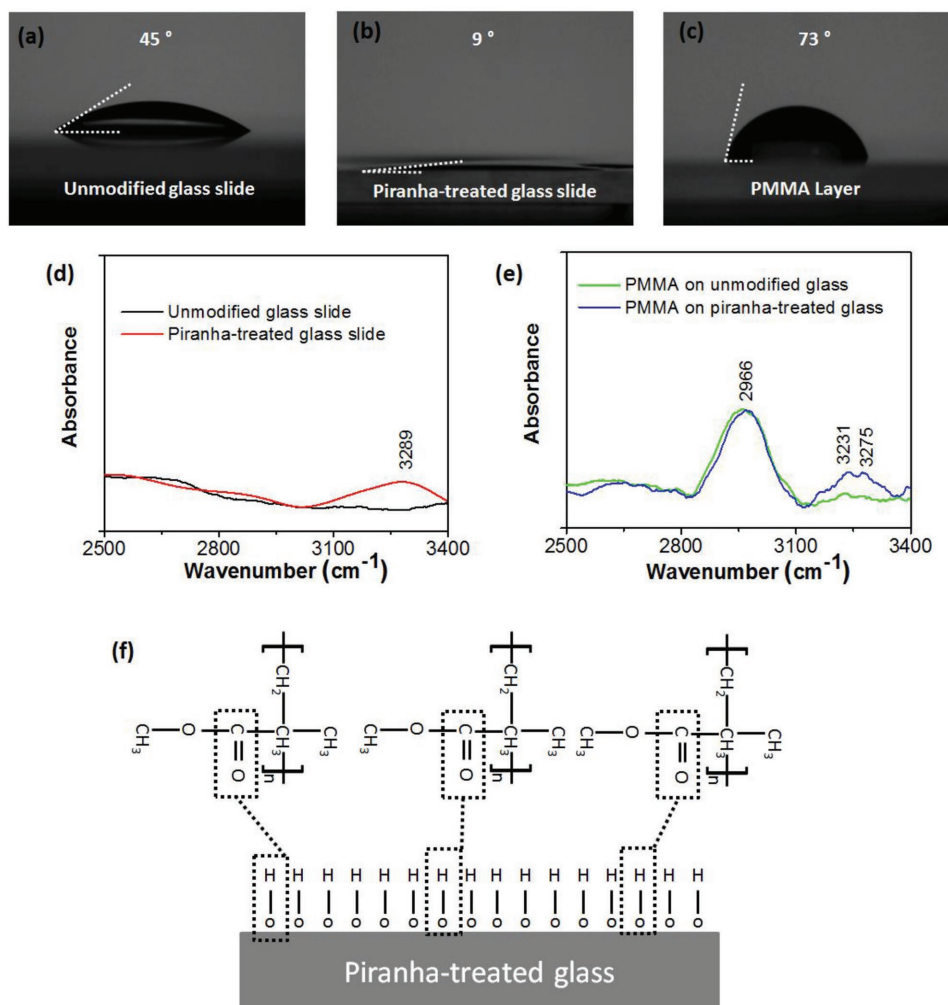


Figure 2. Water contact angle of a) the unmodified glass slide, b) the piranha-treated glass slide, and c) the coated PMMA layer. d) ATR-FTIR spectra at 2500–3400 cm⁻¹ of the unmodified glass slide and the piranha-treated glass slide. e) ATR-FTIR spectra at 2500–3400 cm⁻¹ of the PMMA layer on the unmodified glass slide and the piranha-treated glass slide. f) A schematic depicting the chemical structure of PMMA and the surface of the piranha-treated glass slide. Hydrogen bonding interactions between the carbonyl groups (C=O) in PMMA and the hydroxyl groups (–OH) on the surface of the piranha-treated glass slide are marked with dotted lines.

that hydroxyl groups were generated on the surface during the piranha treatment. For the PMMA on the piranha-treated glass (Figure 2e), the peaks at 2950, 3231, and 3275 cm⁻¹ correspond to the C-H band stretch vibration of PMMA, the associated O-H band vibration at the interface between the PMMA layer and the glass, and the noncomplexed O-H band vibration of glass, respectively.^[45] A schematic explanation of the noncomplexed and associated O-H bands^[46] is given in Figure S2 (Supporting Information). The associated O-H band vibration indicates the formation of hydrogen bonds at the interface between the hydroxyl groups (–OH) of the glass slide and the carbonyl groups (C=O) of PMMA.^[44,45] Figure 2f depicts the hydrogen bonding interfacial interaction between the two groups, resulting in a good adhesion.

In contrast, the peak intensity at 3231 cm⁻¹ was very low or negligible in the case of the PMMA spin-coated on the unmodified glass slide, indicating that there was no strong hydrogen bonding interaction between PMMA and the glass

slide. Therefore, this PMMA layer could be easily separated from the unmodified glass surface. Only Van der Waals interactions were present at the interface. To date, there have been no reports on the use of a PMMA layer as a substrate for electronic devices. Although the Van der Waals interaction is weak, separation without any damage (cracks, holes, rupture, and split) to the PMMA layer was still challenging. Defect-free separation is very crucial when electronic devices are placed on the thin PMMA substrate. In our case, we introduced a droplet of water at the interface between the PMMA/glass. The attractive van der Waals interaction of water with the unmodified glass was much stronger than that with the PMMA layer. Therefore, the water droplet readily smeared into the gap to soak the glass surface, inducing easy separation of the PMMA layer from the glass surface, as shown in Video S1 (Supporting Information). IGZO-based TFTs and H₂ sensors were fabricated on the thin PMMA layer and were subjected to further bending studies.

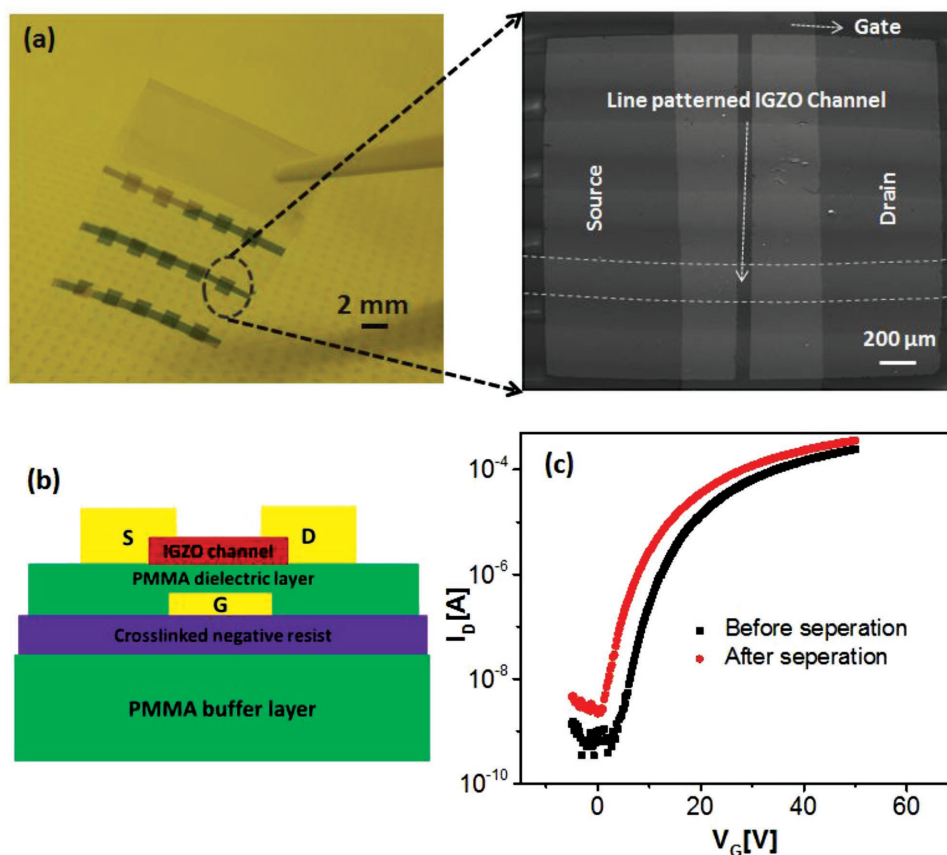


Figure 3. a) A digital image of the flexible bottom-gated IGZO TFTs on the PMMA substrate (left) and a scanning electron microscope (SEM) image of a TFT showing line-patterned IGZO channels (right). b) Schematic cross-sectional view of an IGZO transistor on the flexible PMMA substrate. Dotted lines present a IGZO line channel for eye guide. c) Representative transfer characteristics of the bottom-gated IGZO TFT before and after separation.

2.2. IGZO-Based TFTs on the PMMA Substrate and Their Bending Performance

A digital image of bottom-gated IGZO TFTs and the schematic cross-sectional view of a transistor are shown in **Figure 3a,b**, respectively. If the IGZO was radio frequency (RF)-sputtered under only argon (Ar) gas flow, the current was very high (10^{-2} A) even under no gate bias because of high oxygen vacancies within the as-deposited IGZO film.^[47] Therefore, the IGZO film should be annealed at a temperature above 300 °C under ambient conditions to achieve a low off-current level. However, as the PMMA substrate cannot withstand such a high annealing temperature, oxygen (O_2) gas was introduced along with Ar gas while sputtering the IGZO film for the lowering of the annealing temperature. In this work, the IGZO film was deposited using RF sputtering under Ar and O_2 gas flow rates of 200 and 2 sccm, respectively, and subsequently annealed for 2 h at 120 °C, which is considerably lower than the decomposition temperature of PMMA (241 °C).^[47] The off-current level of the IGZO film was $\approx 10^{-10}$ A. The details of the device fabrication sequence are given in the Experimental Section.

We found that the continuous IGZO film on top of PMMA had unwanted cracks after annealing at 120 °C (see Figure S3a,b, Supporting Information). This is due to the difference in thermal expansion coefficient between the PMMA and

IGZO layers. While annealing at 120 °C, the polymeric chains of PMMA had multiple degrees of freedom and expanded in response to the applied thermal energy. After being cooled, the polymer chains became relaxed and returned back to their original position. However, because the IGZO layer did not expand in the IGZO layer. To avoid those cracks in the IGZO layer, we created 200 μm wide IGZO line channels rather than a bulky IGZO channel. While annealing the line-patterned IGZO/PMMA, the thermal stress from the PMMA layer occurred only at the gaps between the IGZO lines because the PMMA layer underneath the IGZO lines was pinned and bound. Therefore, undesirable cracks in the IGZO line channels were avoided after cooling down to ambient temperature (see Figure S3c,d, Supporting Information). A bottom-gated IGZO TFT with the IGZO line channels had no observable cracks, as shown in Figure 3a.

All the transistor characteristics were measured at room temperature inside a glovebox (nitrogen atmosphere). The transfer characteristics of the bottom-gated IGZO TFT before and after separation are compared in Figure 3c. A small negative shift in threshold voltage was observed after separation. During the separation, the top surface of the IGZO lines was unavoidably in contact with a slight amount of water and experienced a little mechanical stress. It is widely accepted that the water

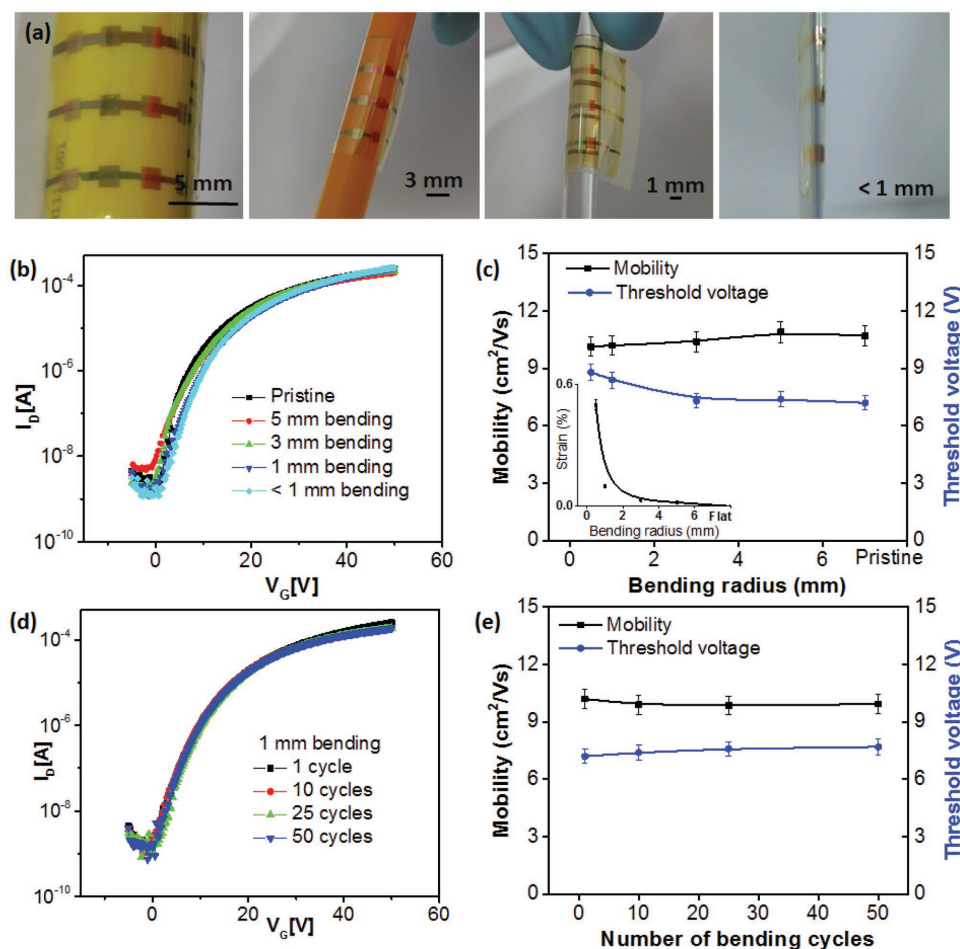


Figure 4. a) Digital images of IGZO TFTs subjected to different bending radii ranging from 5 mm to < 1 mm. b) Their respective transfer characteristics measured after releasing the bending strain. c) Comparison of the mobilities and threshold voltages, which are extracted from the transfer curves in (b). The inset figure presents the bending strain acting on the transistor with respect to the bending radius. d) Transfer characteristics of the IGZO TFTs subjected to different numbers of bending cycles at a 1 mm bending radius and e) the change in mobility and threshold voltage with an increasing number of bending cycles.

molecules absorbed on the IGZO surface supply electron carriers within the channel.^[48,49] Therefore, the electron accumulation at the IGZO/PMMA interface can lower the threshold voltage. A slight increase in the off-current level from 5×10^{-10} to 3×10^{-9} was also observed.

The bottom-gated IGZO TFTs were subjected to bending perpendicular to the channel length direction at different bending radii ranging from 5 to < 1 mm. **Figure 4a** displays digital images of bottom-gated IGZO TFTs subjected to different bending radii of 5, 3, 1, and < 1 mm. The transfer characteristics were measured after releasing the bending strain, as shown in **Figure 4b**. The mobility and threshold voltage were extracted from the transfer curves. The TFTs subjected to different bending radii demonstrated almost similar transistor performance in terms of mobility and threshold voltage (**Figure 4c**). It is commonly known that a decrease in bending radius increases the bending strain of the device, which further affects the transistor performance. However, in our case, the devices demonstrated similar transistor performances even after being subjected to the bending radius < 1 mm, as shown in **Figure 4b,c**.

The bending strain exerted on a flexible device is 100 times the ratio of the substrate thickness to the bending diameter. Therefore, by reducing the substrate thickness, the bending strain exerted on the device can be reduced. Accordingly, by utilizing the ultrathin PMMA substrate (1.9 μm), we demonstrated almost no degradation in transistor performance even after harsh bending treatment at a bending radius of ≈ 0.2 mm, corresponding to a bending strain of 0.475 %, as shown in the inset of **Figure 4c**. For reference, the maximum bending strain reported for metal oxide-based TFTs was 3.33% at a 1.5 mm bending radius (with the use of a 100 μm thick polyimide substrate).^[47] Furthermore, even after 50 bending cycles at a 1 mm bending radius, the bottom-gated IGZO TFT on the thin PMMA substrate demonstrated stable device performance with a mobility of $10.7 \text{ cm}^2 \text{ V}^{-1} \text{ s}^{-1}$, a threshold voltage of 7.2 V and an on/off current ratio of 5×10^5 (**Figure 4d,e**). The IGZO channel surfaces were observed by a scanning electron microscope (SEM) after 1, 10, 25, and 50 bending cycles. The SEM image obtained after 50 bending cycles shows no visible cracks along the line-patterned IGZO channels (see **Figure S4**, Supporting Information).

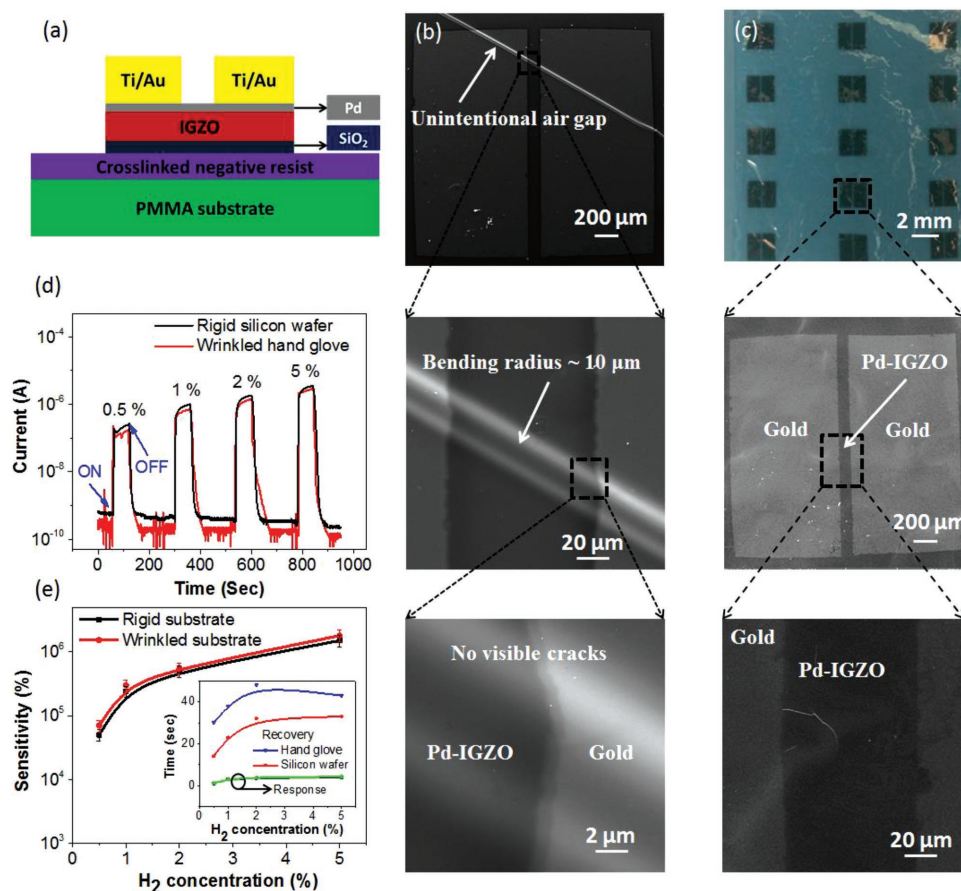


Figure 5. Flexible Pd-dec IGZO H_2 -sensors. a) Schematic cross-sectional view of a Pd-dec IGZO-based H_2 sensor. b) A SEM image and c) a digital image of the Pd-dec IGZO sensor attached to a rigid silicon wafer and a wrinkled hand glove, respectively, along with magnified SEM images. Comparison of H_2 gas sensing performance between the Pd-dec IGZO H_2 sensors placed on a rigid silicon wafer and a wrinkled hand glove at hydrogen concentrations varied from 0.5% to 5%. d) Electrical responses and e) the corresponding sensitivities along with the response and recovery behaviors (inset figure). Two response curves for the two cases are on top of each other.

2.3. IGZO-Based H_2 Sensors on the PMMA Substrate and Their Bending Performance

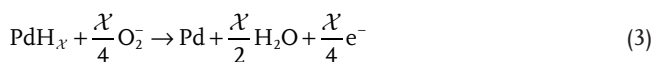
Figure 5a depicts a schematic cross-sectional view of the Pd-dec IGZO H_2 sensor. The sensor was separated from the glass slide and attached to a rigid silicon wafer and a wrinkled hand glove, as shown in Figure 5b,c, respectively. Figure 5c is a magnified image of arrayed H_2 sensors attached to a wrinkled hand glove. We found that an air gap with a curvature radius of $\approx 10 \mu\text{m}$ was unintentionally formed while transferring the thin PMMA substrate having the H_2 sensors to the silicon wafer surface. Interestingly, no visible cracks were observed in the channel and electrode located around the air gap (bottom image of Figure 5b), demonstrating the superior flexibility of the H_2 sensor placed on the thin PMMA substrate.

The Pd-dec IGZO sensor was measured under an ambient air atmosphere with the use of a sensor setup described elsewhere.^[50] The electrical (sensing) responses of the Pd-dec IGZO sensor placed on the rigid silicon wafer or the wrinkled hand glove under different H_2 concentrations ranging from 0.5% to 5% are compared in Figure 5d. In general, metal oxide-based gas sensors require a high operating temperature

(>300 °C) or UV light irradiation to detect H_2 gas. The oxygen molecules in ambient atmosphere are chemisorbed on the metal oxide surface, resulting in electron depletion in the channel (Equation (1)) and thus a low off-current level. These chemisorbed oxygen molecules are too tightly bound to the metal oxide surface at room temperature, and therefore, high activation energy (i.e., high operating temperature) is required to remove the chemisorbed oxygen species from the metal oxide surface.

However, room temperature-operated H_2 gas sensors were demonstrated with a high selectivity toward H_2 gas by using a thin Pd catalytic layer on top of zinc oxide nanowires surface.^[51] In our previous work, we found that a 1 nm thick Pd layer was composed of many tiny Pd islands on an IGZO surface and dramatically enhanced H_2 gas detection at room temperature.^[50] The Pd acts as a catalyst for absorbing and dissociating the H_2 molecules to form palladium hydride (Equation (2)), which can readily react with the chemisorbed oxygen species on the IGZO surface and release water vapor (Equation (3)). The captured electron carriers are then liberated to the IGZO channel. Simultaneously, some of the dissociated H_2 molecules can react with the interstitial oxygens and creates oxygen vacancies in

the IGZO channel (see Figure S5, Supporting Information),^[52] resulting in electron accumulation and thereby abrupt increase in current level (on-current) from 10^{-11} to 10^{-10} A to 10^{-6} A, as shown in Figure 5d



The gas sensor sensitivity, extracted from Figure 5d, was plotted at different hydrogen concentrations, as shown in Figure 5e. The sensors placed on the two different surfaces demonstrated similar sensing performance with the highest sensitivity of $2.3 \times 10^6\%$ as well as fast response (≈ 4 s) and recovery (≈ 43 s) behavior at a 5% H_2 concentration, as shown in the inset of Figure 5e. The sensors placed on a silicon wafer detected H_2 concentration down to 0.05% with a sensitivity of 3% (see Figure S6, Supporting Information).

For the stability test, the Pd-dec IGZO H_2 sensor was subjected to 1 mm bending strain for 1000 cycles and the sensing performance was measured periodically as shown in Figure 6a,b, demonstrating superior repeatable and stable

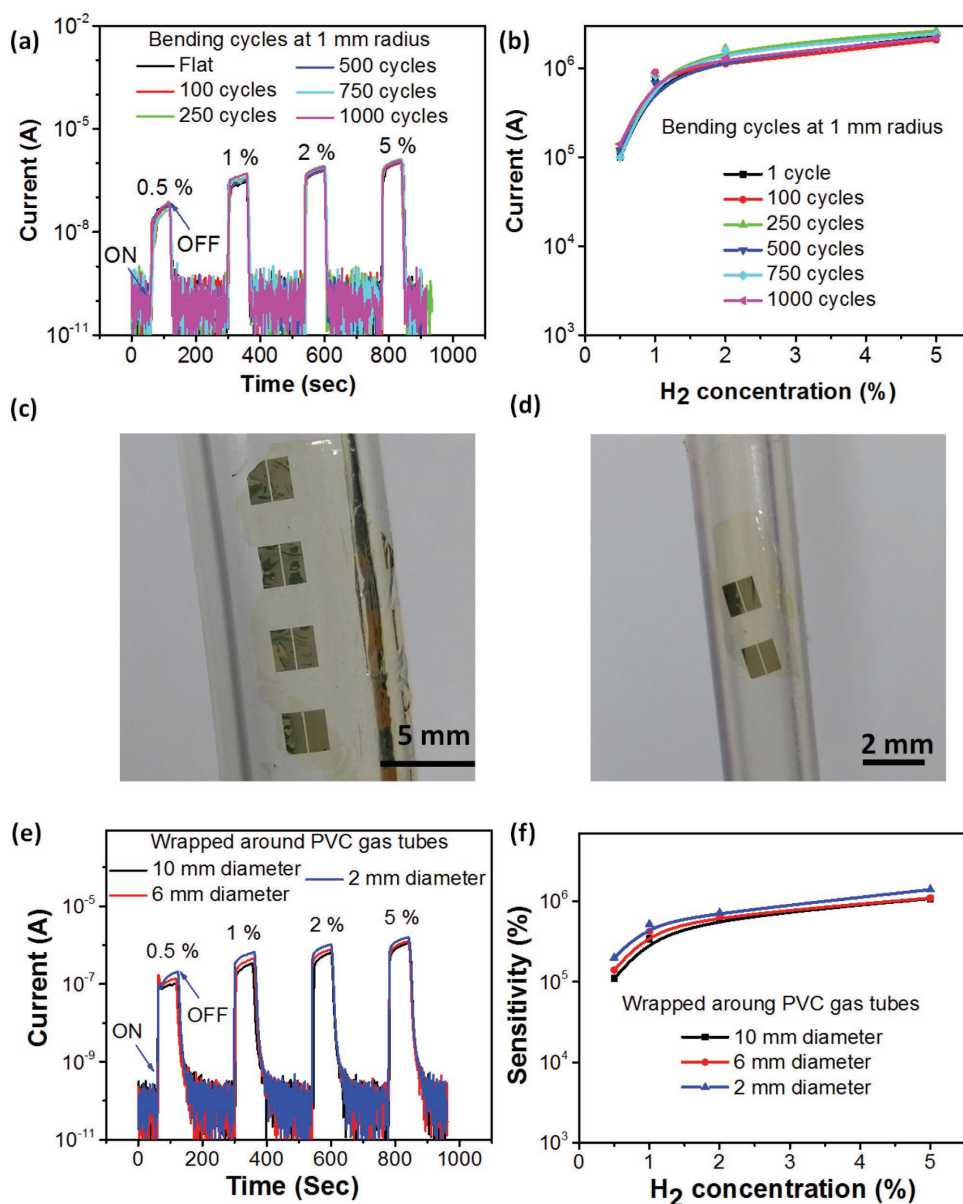


Figure 6. Stability test of the Pd-dec IGZO-based H_2 sensor at a 1 mm bending radius up to 1000 cycles; a) electrical responses and b) the corresponding sensitivities at different H_2 concentrations measured after releasing the bending strain. Images of the Pd-dec IGZO sensors wrapped around PVC gas tubes with diameters of c) 10 mm and d) 2 mm. e) Electrical responses while being wrapped at different bending diameters and f) their corresponding sensitivities.

sensing behavior. The Pd-dec IGZO sensors were also wrapped around different PVC gas tubes with diameters of 10 and 2 mm, as shown in Figure 6c,d, respectively. The electrical responses at different H₂ concentrations varied from 0.5% to 5% were also measured while being wrapped around the PVC gas tubes of different diameters, and the sensors demonstrated almost similar sensing performance with a sensitivity of $1.6 \times 10^6\%$ at a 5% H₂ concentration (Figure 6e). The sensitivity slightly increased with decreasing bending radius (Figure 6f). This is probably due to the slightly increased surface area during the bending treatment, inducing more H₂ gas absorption sites.^[53]

A digital image of a self-coiled sensor just after separation from the glass slide is also shown in Figure S7b (Supporting Information). In this case (bending radius <1 mm), the electrical response was measured after releasing the bending strain, and the sensing performance was as stable as those of the wrapped sensors (see Figure S7c,d, Supporting Information). These free-standing H₂ sensors have the potential to be conformably attached to fittings of containers or pipe lines to detect even small amounts of H₂ leakage and monitor exact leak points in time.

3. Conclusions

In summary, we successfully demonstrated ultraflexibility in metal oxide-based electronic devices on a thin substrate. We utilized 1.9 μm thick PMMA substrate as a flexible substrate, on which bottom-gated IGZO TFTs and Pd-dec IGZO H₂ sensors were produced. The PMMA substrate having the devices was peeled off the glass substrate by engineering the surface energy of the glass. The adhesion of the PMMA layer spin-coated on the unmodified glass slides (fewer hydroxyl groups on the surface) was low enough for easy separation of the PMMA layer from the glass slide surface. The bottom-gated IGZO TFTs on the thin PMMA substrate demonstrated stable transistor performance even after 50 bending cycles at a 1 mm bending radius with a mobility of $10.7 \text{ cm}^2 \text{ V}^{-1} \text{ s}^{-1}$, a threshold voltage of 8.4 V and an on/off current ratio of 5×10^5 . In addition, the Pd-dec IGZO H₂ sensors on the PMMA substrate could attach to wrinkled hand gloves through a photocurable polymer or wrap around PVC gas tubes with the use of glue. The H₂ sensors demonstrated an excellent sensitivity of $1.6 \times 10^6\%$ at a 5% H₂ concentration at room temperature even after exposure to harsh bending treatment at a bending radius <1 mm. Both electronic devices placed on the thin PMMA substrate demonstrated an unprecedented flexibility without any performance degradation, indicating that they can be applied to future wearable and portable electronics.

4. Experimental Section

Preparation of PMMA Substrate: (Figure S8, Supporting Information) Ultrathin PMMA substrates were prepared by spin-coating a 1.2 μm thick PMMA layer on a rigid unmodified glass slide and was annealed at 130 °C for 2 h. As the ultrathin PMMA was highly fragile due to its soft nature, 0.7 μm thick Clariant nLOF 2020 (negative resist) was spin-coated as a supporting and barrier layer on the PMMA surface and annealed at 115 °C for 2 min. The stability of the negative photoresist

was improved by UV exposure and subsequent postannealing at 130 °C for 2 h. After fabrication of the TFTs and H₂ sensors on the negative resist, the PMMA substrate having the fabricated devices was readily peeled off the rigid glass slide by placing a tiny water drop at the interface between the glass slide and PMMA layer (see Video S1, Supporting Information).

Fabrication of TFTs on the Ultrathin PMMA Substrate: Bottom-gated IGZO TFTs were fabricated on the 1.9 μm thick (negative resist/PMMA) substrate coated on a rigid glass slide, as shown in Figure S9a (Supporting Information). To enhance the adhesion of gate electrode to the negative resist layer, oxygen plasma treatment was performed on the negative resist layer prior to gate electrode deposition. A 50 nm thick gate electrode (Au/Ti) was then electron-beam (e-beam) deposited using a shadow mask with dimensions of a 0.6 mm width and a 3 cm length. A 0.8 μm thick PMMA gate dielectric layer was spin-coated on top of the gate electrode and annealed at 130 °C for 2 h. After a 30 s oxygen plasma treatment for adhesion enhancement, 50 nm thick IGZO active lines were deposited by RF sputtering through a shadow mask (200 μm line width) by using an IGZO target (In₂O₃:Ga₂O₃:ZnO = 1:1:1 atomic ratio) under a chamber pressure of 5 mTorr with O₂ and Ar flow rate of 2 and 200 sccm, respectively. Subsequently, 50 nm thick source and drain (S/D) electrodes (Au/Ti) were e-beam deposited using a shadow mask with a channel length and width of 100 μm and 2 mm, respectively. To achieve good contact between the channel and contact electrodes, the whole device was annealed at 120 °C for 2 h under air atmosphere. Finally, the flexible bottom-gated IGZO TFTs on the ultrathin PMMA substrate were obtained by separating the PMMA layer from the rigid glass slide.

Fabrication of H₂ Sensors on the Ultrathin PMMA Substrate: IGZO-based H₂ sensors were also fabricated on the 1.9 μm thick PMMA substrate, as shown in Figure S9b (Supporting Information). To attain low moisture permeability, a 20 nm thick SiO₂ layer was e-beam deposited through a shadow mask with a width and length of 3 and 5 mm, respectively. A 50 nm thick IGZO layer was deposited on top of the SiO₂ surface as described above. A 1 nm thick Pd layer was then deposited on the IGZO layer by e-beam deposition. Subsequently, 50 nm thick contact electrodes (Au/Ti) were e-beam deposited using a shadow mask with a channel length and width of 100 μm and 2 mm, respectively. The PMMA layer having the IGZO-based H₂ sensors was then peeled off the rigid glass slide. To attach the H₂ sensors on a wrinkled hand glove, first, a photocurable polymer was coated on the hand glove by doctor blade technique (see Figure S10b, Supporting Information). The photocurable polymer was formulated by mixing a siliconized urethane acrylate oligomer (CN990) and 2,2-dimethoxy-2-phenylacetophenone (photoinitiator) in an optimized weight ratio of 1:0.015. The conformal adhesion of the IGZO-based H₂ sensors to the wrinkled hand glove was achieved after UV curing, as shown in Figure 5c.

Supporting Information

Supporting Information is available from the Wiley Online Library or from the author.

Acknowledgements

This work was supported by the Pioneer Research Center Program (No. NRF-2016M3C1A3908893) and by the Basic Science Research Program (No. NRF-2016R1A2B4006395) through the National Research Foundation of Korea (NRF) funded by the Ministry of Science and ICT. The research was partially supported by the GIST Research Institute (GRI) project through a grant provided by GIST in 2018.

Conflict of Interest

The authors declare no conflict of interest.

Keywords

flexible electronics, hydrogen gas sensors, indium-gallium-zinc oxide (IGZO), surface energy, transistors, ultrathin substrates

Received: March 19, 2018

Revised: April 15, 2018

Published online: May 31, 2018

- [1] W. Gao, S. Emaminejad, H. Y. Y. Nyein, S. Challa, K. Chen, A. Peck, H. M. Fahad, H. Ota, H. Shiraki, D. Kiriya, D.-H. Lien, G. A. Brooks, R. W. Davis, A. Javey, *Nature* **2016**, 529, 509.
- [2] X. Pu, L. Li, M. Liu, C. Jiang, C. Du, Z. Zhao, W. Hu, Z. L. Wang, *Adv. Mater.* **2016**, 28, 98.
- [3] M. Amjadi, K.-U. Kyung, I. Park, M. Sitti, *Adv. Funct. Mater.* **2016**, 26, 1678.
- [4] S. Choi, H. Lee, R. Ghaffari, T. Hyeon, D.-H. Kim, *Adv. Mater.* **2016**, 28, 4203.
- [5] J. Kim, J. Lee, D. Son, M. K. Choi, D.-H. Kim, *Nano Convergence* **2016**, 3, 4.
- [6] Y.-B. Yin, X.-Y. Yang, Z.-W. Chang, Y.-H. Zhu, T. Liu, J.-M. Yan, Q. Jiang, *Adv. Mater.* **2018**, 30, 1703791.
- [7] X.-Y. Yang, J.-J. Xu, D. Bao, Z.-W. Chang, D.-P. Liu, Y. Zhang, X.-B. Zhang, *Adv. Mater.* **2017**, 29, 1700378.
- [8] Q.-C. Liu, T. Liu, D.-P. Liu, Z.-J. Li, X.-B. Zhang, Y. Zhang, *Adv. Mater.* **2016**, 28, 8413.
- [9] T. Liu, Q.-C. Liu, J.-J. Xu, X.-B. Zhang, *Small* **2016**, 12, 3101.
- [10] T. Liu, J.-J. Xu, Q.-C. Liu, Z.-W. Chang, Y.-B. Yin, X.-Y. Yang, X.-B. Zhang, *Small* **2017**, 13, 1602952.
- [11] S. Gong, D. T. H. Lai, B. Su, K. J. Si, Z. Ma, L. W. Yap, P. Guo, W. Cheng, *Adv. Electron. Mater.* **2015**, 1, 1400063.
- [12] S. Bai, C. Sun, P. Wan, C. Wang, R. Luo, Y. Li, J. Liu, X. Sun, *Small* **2015**, 11, 306.
- [13] P. Wan, X. Wen, C. Sun, B. K. Chandran, H. Zhang, X. Sun, X. Chen, *Small* **2015**, 11, 5409.
- [14] S. Bai, C. Sun, H. Yan, X. Sun, H. Zhang, L. Luo, X. Lei, P. Wan, X. Chen, *Small* **2015**, 11, 5807.
- [15] C. S. Luo, P. Wan, H. Yang, S. A. A. Shah, X. Chen, *Adv. Funct. Mater.* **2017**, 27, 1606339.
- [16] E. G. Bittle, J. I. Basham, T. N. Jackson, O. D. Jurchescu, D. J. Gundlach, *Nat. Commun.* **2016**, 7, 10908.
- [17] Z. Wang, P. K. Nayak, J. A. Caraveo-Frescas, H. N. Alshareef, *Adv. Mater.* **2016**, 28, 3831.
- [18] R. Adzhri, M. K. Md Arshad, S. C. B. Gopinath, A. R. Ruslinda, M. F. M. Fathil, R. M. Ayub, M. N. M. Nor, C. H. Voon, *Anal. Chim. Acta* **2016**, 917, 1.
- [19] J.-H. Lee, J.-Y. Kim, J.-H. Kim, A. Mirzaei, H. W. Kim, S. S. Kim, *Nano Convergence* **2017**, 4, 27.
- [20] H. Yan, M. J. Zhong, Z. Lv, P. B. Wan, *Small* **2017**, 13, 1701697.
- [21] P. Heremans, A. K. Tripathi, A. d. J. d. Meux, E. C. P. Smits, B. Hou, G. Pourtois, G. H. Gelinck, *Adv. Mater.* **2016**, 28, 4266.
- [22] T. Wang, Y. L. Guo, P. B. Wan, X. D. Chen, X. M. Sun, *Small* **2016**, 12, 3748.
- [23] S. Mousavi, K. Kang, J. Park, I. Park, *RSC Adv.* **2016**, 6, 104131.
- [24] O. Krsko, T. Plecenik, T. Roch, B. Grancic, L. Satrapinsky, M. Truchly, P. Durina, M. Gregor, P. Kus, A. Plecenik, *Sens. Actuators, B* **2017**, 240, 1058.
- [25] C. Kuru, D. Choi, A. Kargar, C. H. Liu, S. Yavuz, C. Choi, S. Jin, P. R. Bandaru, *Nanotechnology* **2016**, 27, 195501.
- [26] A. Pecora, L. Maiolo, M. Cuscuna, D. Simeone, A. Minotti, L. Mariucci, G. Fortunato, *Solid-State Electron.* **2008**, 52, 348.
- [27] K. Hassan, A. S. M. I. Uddin, F. Ullah, Y. S. Kim, G.-S. Chung, *Mater. Lett.* **2016**, 176, 232.
- [28] Y. Hu, C. Warwick, A. Sou, L. Jiang, H. Sirringhaus, *J. Mater. Chem. C* **2014**, 2, 1260.
- [29] D. Ji, A. D. Donner, G. Wilde, W. Hu, H. Fuchs, *RSC Adv.* **2015**, 5, 98288.
- [30] X. Wu, Y. Ma, G. Zhang, Y. Chu, J. Du, Y. Zhang, Z. Li, Y. Duan, Z. Fan, J. Huang, *Adv. Funct. Mater.* **2015**, 25, 2138.
- [31] K. Fukuda, T. Sekine, R. Shiwaku, T. Morimoto, D. Kumaki, S. Tokito, *Sci. Rep.* **2016**, 6, 27450.
- [32] L. Zhang, H. Wang, Y. Zhao, Y. Guo, W. Hu, G. Yu, Y. Liu, *Adv. Mater.* **2013**, 25, 5455.
- [33] A. Maliakal, K. Raghavachari, H. Katz, E. Chandross, T. Siegrist, *Chem. Mater.* **2004**, 16, 4980.
- [34] O. D. Jurchescu, J. Baas, T. T. M. Palstra, *Appl. Phys. Lett.* **2004**, 84, 3061.
- [35] X. Yu, T. J. Marks, A. Facchetti, *Nat. Mater.* **2016**, 15, 383.
- [36] M. Pesic, F. P. G. Fengler, L. Larcher, A. Padovani, T. Schenk, E. D. Grimley, X. Sang, J. M. LeBeau, S. Slesazek, U. Schroeder, T. Mikolajick, *Adv. Funct. Mater.* **2016**, 26, 4601.
- [37] D. Fu, C. Zhu, X. Zhang, C. Lia, Y. Chen, *J. Mater. Chem. A* **2016**, 4, 1390.
- [38] J. A. Rogers, T. Someya, Y. Huang, *Science* **2010**, 327, 1603.
- [39] M. J. Han, D.-Y. Khang, *Adv. Mater.* **2015**, 27, 4969.
- [40] K. Hassan, A. S. M. I. Uddin, G.-S. Chung, *Sens. Actuators B* **2016**, 234, 435.
- [41] Y.-H. Kim, E. Lee, J. G. Um, M. Mativenga, J. Jang, *Sci. Rep.* **2016**, 6, 25734.
- [42] M. Mativenga, D. Geng, B. Kim, J. Jang, *ACS Appl. Mater. Interfaces* **2015**, 7, 1578.
- [43] K. Park, D.-K. Lee, B.-S. Kim, H. Jeon, N.-E. Lee, D. Whang, H.-J. Lee, Y. J. Kim, J.-H. Ahn, *Adv. Funct. Mater.* **2010**, 20, 3577.
- [44] G. Mallikarjunachari, P. Ghosh, *Polymer* **2016**, 90, 53.
- [45] V. Janarthanan, G. Thyagarajant, *Polymer* **1992**, 33, 3593.
- [46] J. T. Reilly, A. Thomas, A. R. Gibson, C. Y. Luebehusen, M. D. Donohue, *Ind. Eng. Chem. Res.* **2013**, 52, 14456.
- [47] Y. Kumaresan, Y. Pak, N. Lim, Y. Kim, M.-J. Park, S.-M. Yoon, H.-M. Youn, H. Lee, B. H. Lee, G. Y. Jung, *Sci. Rep.* **2016**, 6, 37764.
- [48] J.-S. Park, J. K. Jeong, H.-J. Chung, Y.-G. Mo, H. D. Kim, *Appl. Phys. Lett.* **2008**, 92, 072104.
- [49] J. K. Jeong, H. W. Yang, J. H. Jeong, Y.-G. Mo, H. D. Kim, *Appl. Phys. Lett.* **2008**, 93, 123508.
- [50] Y. Kumaresan, H. Kim, Y. Jeong, Y. Pak, S. Cho, R. Lee, N. Lim, G. Y. Jung, *IEEE Electron Device Lett.* **2017**, 38, 1735.
- [51] H. Kim, Y. Park, Y. Jeong, W. Kim, J. Kim, G. Y. Jung, *Sens. Actuators, B* **2018**, 262, 460.
- [52] N. J. Dayan, S. R. Sainkar, R. N. Karekar, R. C. Aiyery, *Meas. Sci. Technol.* **1998**, 2, 360.
- [53] T.-R. Rashid, D.-T. Phan, G.-S. Chung, *Sens. Actuators, B* **2013**, 185, 777.